Journal of Membrane Science 369 (2011) 49–58

Contents lists available at ScienceDirect

Journal of Membrane Science

journal homepage: www.elsevier.com/locate/memsci

Gas permeation properties of poly(urethane-urea)s containing different polyethers

Hua Li[a], Benny D. Freeman[a,*], O. Max Ekiner[b]

[a] The University of Texas at Austin, Department of Chemical Engineering, Center for Energy and Environmental Resources, 10100 Burnet Road, Building 133, Austin, TX 78758, United States
[b] Air Liquide, Delaware Research and Technology Center, 200 GBC Drive, Newark, DE 19702, United States

ARTICLE INFO

Article history:
Received 2 June 2010
Received in revised form 29 October 2010
Accepted 11 November 2010
Available online 18 November 2010

Keywords:
Poly(urethane-urea)
Carbon dioxide
Polymer membranes
Separation
Permeability
Permeation properties
Transport

ABSTRACT

A series of poly(urethane-urea)s were synthesized using 4,4′-methylenediphenyl diisocyanate (MDI), various polyether diols, and ethylene diamine (EDA). The polyethers were poly(ethylene glycol) (PEG) 2000, poly(propylene glycol) (PPG) 2700, poly(tetramethylene ether glycol) (Terathane®) 2000, Terathane® 2900, and a mixture of PEG 2000 and Terathane® 2000. The polymer based on PEG 2000 is semi-crystalline at room temperature, and the others are amorphous. The fractional free volume (FFV) increases as polyether molecular weight and soft segment content increase. The permeability of these materials to He, H_2, O_2, N_2, CO_2 and CH_4 was measured at 35 °C, and gas permeability increased with increasing FFV. The physical properties and gas transport characteristics of these poly(urethane-urea)s were compared with those of rubbery networks based on crosslinked PEG and PPG.

1. Introduction

Polyurethanes and poly(urethane-urea)s are linear block copolymers composed of flexible and rigid segments [1]. They usually have a micro-phase separated structure due to the incompatibility between the soft and hard segments [2]. The gas transport performance is affected by the concentration as well as the chemical structures of the hard and soft segments [3–5]. Generally, gas permeability of polyurethane membranes increases as polyether diol molecular weight increases (i.e., as soft segment content increases) [5]. The effect of hard-segment content on gas separation properties has also been explored [6].

Gas separation using polymeric membranes has attracted significant interest in recent decades because it can be more energy-efficient than other separation techniques [7–9]. Among gas separation applications, interest has increased in membranes for CO_2 gas separation due to the wide variety of potential applications [10], such as CO_2/H_2 separation in synthesis gas purification, CO_2/N_2 in carbon capture, CO_2/CH_4 in natural gas purification, and CO_2/O_2 in food packaging [10–12]. Poly(ethylene oxide) (PEO) has been identified as having interesting gas separation properties, particularly for polar, quadrupolar, or acid gas (e.g., CO_2, H_2S) removal from non-polar gases (e.g., H_2, N_2, and CH_4) [10,13,14]. The polar ether oxygen in PEO interacts favorably with CO_2 molecules, which contributes to high selectivity towards CO_2 by membranes containing sufficient amounts of PEO [10]. Based on these composite characteristics, PEO has been used in many material platforms for CO_2-based gas separations, such as crosslinked PEO [13,15–18], Pebax [19–22], PEO-polyester [23,24], PEO-PI [25,26] and PEO blends [27].

In many applications of interest, water is also present. However, PEO is water-sensitive, and linear, uncrosslinked PEO is, in fact, water soluble. In preparing membranes for gas separation applications, materials with good humidity resistance and favorable gas separation properties are of interest. In this regard, poly(tetramethylene ether glycol) (Terathane®) and poly(propylene glycol) (PPG) both have ether structures similar to that of PEO and may interact with CO_2, leading to high CO_2 solubility in the polymer. However, they are more hydrophobic than PEO and so may have better stability in humid environments than PEO-based materials. Additionally, the gas transport properties of such materials have been less thoroughly studied than those of PEO-based systems. Therefore, in this study, similar molecular weights of PPG and Terathane® were used as soft segments, and the effect of chemical structure on gas permeability in these poly(urethane-urea)s was studied. Control materials based on PEO were also synthesized for comparison.

* Corresponding author. Tel.: +1 512 232 2803; fax: +1 512 232 2807.
E-mail address: freeman@che.utexas.edu (B.D. Freeman).

0376-7388/$ – see front matter © 2010 Elsevier B.V. All rights reserved.
doi:10.1016/j.memsci.2010.11.024

2. Experimental

2.1. Materials

All chemicals were purchased from Sigma–Aldrich. 4,4′-Methylenebis(phenyl isocyanate) (MDI) was purified by vacuum distillation before use. Poly(ethylene glycol) (PEG, M_w = 2000), poly(propylene glycol) (PPG, M_w = 2700) and poly(tetramethylene ether glycol) (Terathane®, M_w = 2000 and 2900) were vacuum dried at 90 °C for 8 h before use. Ethylene diamine and diethylamine were vacuum distilled before use. The catalyst, dibutyltin dilaurate (DBTDL), was used as received. *N*,*N*-Dimethyl acetamide (DMAc) was refluxed with CaH_2 for more than 3 h, then distilled, and the overhead product obtained between 156 and 157 °C was collected. Methanol was used as received. Gas cylinders of methane with 99% chemical purity and UHP level (i.e., 99.999%) helium, nitrogen, oxygen, hydrogen and carbon dioxide were purchased from Airgas Southwest Inc. (Corpus Christi, TX) and used as received.

Polyether molecular weights were determined prior to synthesis by hydroxyl (OH) group titration using ASTM D 4274-05, Method C [28]. Hydroxyl groups react with excess phthalic anhydride; the unreacted anhydride was back titrated using dilute sodium hydroxide solution. The isocyanate content in monomers and prepolymers was determined using ASTM D 5155-01, Method B [29]. Isocyanate groups react with excess dibutyl amine, and the unreated amine was back titrated using dilute hydrochloric acid.

2.2. Polymer synthesis and membrane preparation

The basic scheme of the polymer synthesis is presented in Fig. 1. For example, 20.21 g (0.010 mol) of Terathane® 2000 and 120 ml of *N*,*N*-dimethylacetamide (DMAc) were charged to a 500 ml three-necked flask equipped with mechanical stirrer, a dropping funnel, and a nitrogen outlet. The mixture was stirred under the protection of nitrogen until the Terathane® was totally dissolved. At room temperature, 5.50 g (0.022 mol) of MDI, dissolved in 30 ml of DMAc, were added to the Terathane®/DMAc solution dropwise over a 5-min period. The solution was slowly heated to 90 °C and held at this temperature for 2 h under nitrogen. Afterwards, the solution was cooled to room temperature. Then, 0.66 g (0.011 mol) of EDA, dissolved in 20 ml of DMAc, was added to the solution dropwise under mechanical stirring. The amount of added chain extender (i.e., EDA) did not reach its stoichiometric endpoint (i.e., 0.012 mol) because the polymerization mixture had already become too viscous to be easily stirred using the mechanical stirrer. The solution was then held at 40 °C for 2 h under a nitrogen atmosphere. Excess diethylamine (0.20 g, 0.003 mol) was then added to react with the remaining N=C=O groups and terminate the polymer chains, and the reaction was continued for two more hours at 40 °C in nitrogen. The solution was monitored by FTIR until no N=C=O absorption peak (2200 cm^{-1}) was detected. The reaction was then stopped, and the solution was allowed to cool to room temperature.

After cooling, the polyurethane solution was coagulated by slowly pouring it into 1 L of methanol (i.e., 5 times the volume of the reaction mixture) under stirring, and white precipitated polymer strings were obtained. The precipitated polymer was left in methanol overnight and then cut into small pieces using a blender. The polymer pieces were filtered and washed again with methanol. The resulting polymer was dried at room temperature in air overnight, then in a vacuum oven at 140 °C for 48 h to remove residual DMAc.

In other syntheses, Terathane® 2900, PEG 2000, PPG 2700, and a PEG 2000/Terathane® 2000 mixture (1:1 mixture by weight) were used instead of Terathane® 2000. In each synthesis, 0.010 mol of diol (e.g., 29.0 g of Terathane® 2900) was used. The other reagent amounts and synthesis steps remained the same as indicated above. It has been reported that in PEO-PBT multi-block copolymer membranes, the highest CO_2 permeability was observed when PEO block has a molecular weight between 2000 and 2500 g mol^{-1} [30]. Therefore, to achieve high CO_2 permeability, PEG and other polyether glycols with similar molecular weights were used in our polymer synthesis. Table 1 shows the chemical structure of polyether diols and the soft segment weight fractions in the resulting polymers. Samples containing PPG 2700, Terathane® 2900, Terathane® 2000, mixed PEG 2000/Terathane® 2000, and PEG 2000 were labeled as I, II, III, IV and V, respectively. These identifiers are used in the following discussion.

Poly(urethane-urea) films were prepared from a DMAc solution using a solution casting method. Polyurethanes were dissolved in DMAc at 20 wt% solids and then passed through a filter with 5 μm pores under pressure. The filtered solution was cast, to form a film, onto a glass plate preheated to 80 °C and then vacuum dried at 100 °C for 6 h to remove most of the DMAc, then at 160 °C for 2 h to further remove DMAc. The film was then cooled to room temperature in vacuum and detached from the glass plate. Because of its high polarity, even rigorous drying protocols may not be sufficient to remove all of the residual DMAc, and the presence of such residual solvent may influence permeability measurement results. Therefore, in addition to the drying protocol described above, the films were then solvent exchanged by soaking overnight in a large excess of ethanol. DMAc and ethanol are miscible, and ethanol can swell the polymer samples but not dissolve them. Thus, any DMAc left in the film can solvent exchange with the ethanol when the film swelled. Afterwards, the film was dried in air until most of the ethanol evaporated, then dried in vacuum at 160 °C for 6 h to remove all remaining traces of ethanol. As will be discussed, the removal of residual DMAc and ethanol from the film was confirmed by TGA because no related weight loss was observed. Membrane thickness was measured using a Mitutoyo Litematic VL-50A measuring instrument (Mitutoyo Corporation, Japan). This thickness gauge is specifically designed for use with soft materials, such as rubbery polymers, and employs a low-force micrometer to measure thickness. The thickness of the dry films varied from 80 to 130 μm.

2.3. Density

Film density was characterized using a Mettler Toledo Balance (Model AG204) and a density kit. The film density was calculated as follows [31]:

$$\rho_p = \frac{M_A}{M_A - M_L} \cdot \rho_0 \quad (1)$$

where M_A is the film weight in air, M_L is the film weight in the auxillary liquid, and ρ_0 is the density of the auxillary liquid used. To reduce the sorption of the auxillary liquid in polymer and increase the density difference between the polymer sample and the auxillary liquid, a high density perfluorinated auxillary liquid was used. The perfluoro-alkane FC-77, purchased from Acros Organics, has a density of 1.766 g/cm^3 at 25 °C [32]. This liquid sorbs to a negligible extent in the polymers of interest in this study.

2.4. FTIR-ATR

Attenuated total reflection Fourier transform infrared spectroscopy (FTIR-ATR) was performed using a Thermo Nicolet Nexus 470 FT-IR spectrophotometer (Madison, WI) equipped with an ATR Smart Avatar Miracle attachment (Zinc Selenide crystal). The measurements were conducted at 1 cm^{-1} nominal resolution, 256 scans, and the region from 675 to 4000 cm^{-1} was recorded for each

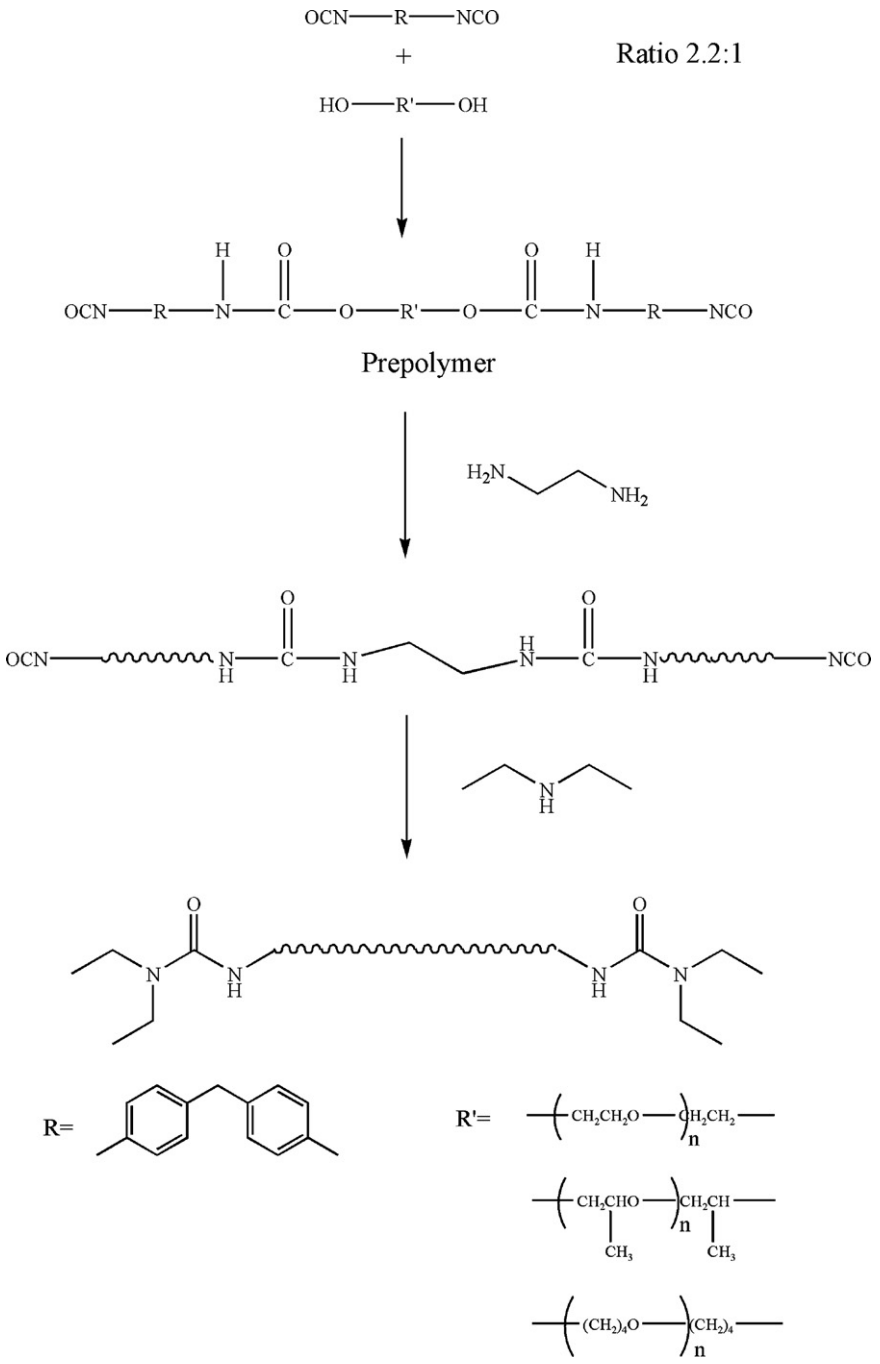

Fig. 1. The chemical structures and synthesis steps used to prepare poly(urethane-urea)s.

spectrum. The data were collected and analyzed using Omnic software from the spectrometer manufacturer.

2.5. Thermal characterization

TGA analysis was conducted using a TGA Q500 V 6.3 equipped with a standard furnace (TA Instruments, New Castle, DE). A sample weighing about 10 mg was loaded into a platinum pan and heated from 25 °C to 800 °C at 5 °C/min in nitrogen gas (flow rate 40 ml/min). Thermal transitions were characterized using a Q100 differential scanning calorimeter (DSC) equipped with a liquid nitrogen cooling system (LNCS) (TA Instruments, New Castle, DE). Polymer samples for DSC analysis weighed 6–10 mg. Samples were placed in aluminum DSC pans, and helium, flowing at 25 ml/min, was used as the blanketing gas in the DSC. The DSC sweep began by taking the sample from ambient to −150 °C and then holding at −150 °C for 5 min to equilibrate and stabilize the system. Then, the sample was scanned from −150 to +250 °C at a heating rate of 10 °C/min. The glass transition temperature (T_g) was taken as the midpoint of the measured step change in heat capacity. The degree of crystallinity was evaluated from the area under the melting endotherm in the scan. DSC and TGA data were analyzed using the Universal Analysis 2000 software provided by TA Instruments.

Wide angle X-ray diffraction (WAXD) was performed at room temperature using a Scintag X1 theta–theta diffractometer, with a Cu Kα radiation of 1.54 Å wavelength (power settings of 45 kV and 50 mA) and a solid state (Si(Li)) detector. The software used for data processing was Jade v. 7.5, Materials Data Inc. (Livermore, CA).

Table 1
Composition of the different polyurethane/polyurea block copolymers and their physical properties.

Sample code	Diol	Soft segment chemical structure	Soft segment content (wt%)	Water uptake (wt%)
I	PPG 2700	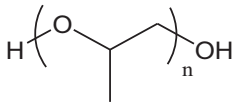	83.1	17 ± 2
II	Terathane® 2900	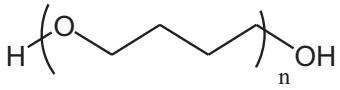	84.3	10 ± 1
III	Terathane® 2000	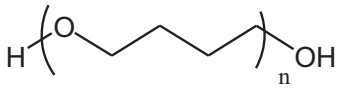	78.4	11 ± 1
IV	Terathane® 2000:PEG 2000 = 1:1		78.4	34 ± 2
V	PEG 2000	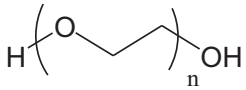	78.4	132 ± 9

2.6. Permeation measurements

The permeability coefficients of N_2, O_2, H_2, He, CH_4 and CO_2 were measured at 35 °C using a constant volume/variable pressure apparatus [20]. The pure gas permeability coefficients are reported in units of Barrer, where 1 Barrer = 10^{-10} cm^3(STP) cm/(cm^2 s cm Hg). Poly(urethane-urea) films obtained from solution casting were first cut to size using a circular die. Impermeable aluminum tape (with an opening in the center to permit gas permeation during the experiment) was then applied to both sides of the film. After a film was mounted in the system, vacuum was applied on both upstream and downstream sides to degas the film. The leak rate was measured before the permeation experiment by sealing both the upstream and downstream volumes when they were still under vacuum and measuring the resulting rate of pressure rise in the downstream volume. The permeability of the sample was calculated as follows [20]:

$$P_A = \frac{Vl}{p_1 ART}\left[\left(\frac{dp_2}{dt}\right)_{ss} - \left(\frac{dp_2}{dt}\right)_{leak}\right] \quad (2)$$

where V is the downstream volume (cm^3), l is the film thickness (cm), p_1 is the upstream absolute pressure (cm Hg), A is the film area (cm^2), T is absolute temperature (K), R is the gas constant (0.278 cm Hg cm^3/(cm^3(STP) K)), and $(dp_2/dt)_{ss}$ and $(dp_2/dt)_{leak}$ are the pseudo-steady state rates of pressure rise in the downstream volume during measurement of a sample and during leak rate measurements (cm Hg/s), respectively. The leak rate was typically less than 10% of the steady state rate of pressure rise during a permeability measurement. All measurements were taken at downstream pressures less than 10 Torr, which was much lower than the upstream pressure, which varied from 3 to 15 atm. The ideal permeability selectivity of a polymer for penetrant gas A relative to gas B is defined as the ratio of the pure gas permeability coefficients of the two gases [20]:

$$\alpha_{A/B} = \frac{P_A}{P_B} \quad (3)$$

2.7. Water uptake

Water uptake was measured by a liquid sorption method [33,34]. Samples were soaked in deionized water at ambient conditions for several days until the swollen film weight stabilized. Before weighing, a film was blotted between two filter papers, and then its mass was recorded with an analytical balance. To obtain the dry mass, the sample was dried in vacuum at 80 °C until its mass did not change. The water uptake (g H_2O/100 g dry polymer) in a film was calculated as follows:

$$W = \frac{M_{swollen} - M_{dry}}{M_{dry}} \times 100 \quad (4)$$

3. Results and discussion

3.1. Polymer characterization

The chemical structures of the poly(urethane-urea)s were verified using FTIR spectroscopy. The amide (–NH) structure in urethane/urea linkages was observed at 3330 cm^{-1} in each spectrum. Peaks between 1730 cm^{-1} and 1710 cm^{-1} correspond to the free carbonyl groups and H-bonded urethane carbonyl groups [35]. The peak around 1645 cm^{-1} correspond to the H-bonded urea carbonyl groups [35]. C–N–H bending in the urethane linkages can be observed around 1545 cm^{-1} [36]. Due to the high molecular weight and high soft segment content (between 78% and 84%), a strong sharp peak appears around 1095 cm^{-1} that is ascribed to the C–O–C stretching of the ether group in polyethers [37]. The 2200–2400 cm^{-1} region remained clear, demonstrating that no unreacted isocyanate groups remained [38]. The detailed FTIR spectra are presented in Supplementary Information for brevity.

TGA was used to investigate the thermal stability of these poly(urethane-urea)s and to verify the absence of solvent in the samples. There was no indication of any mass loss that could be ascribed to the loss of solvent, so the drying protocol has likely removed all solvent from the polymers. All TGA analysis show similar weight loss, which began between 200 °C and 250 °C, indicating the onset of polymer decomposition. The H-bonded urea linkages were suggested to provide improved better thermal stability in poly(urethane-urea)s relative to polyurethanes [39,40]. However, thermal degradation following breaking of H-bonds should not cause weight loss in these poly(urethane-urea)s because the H-bond dissociation temperature is much lower (no more than 130 °C) [41]. The thermal degradation in MDI-based poly(urethane-urea)s was suggested to start with cleavage of N–H and C–H bonds in the hard segments [42], and the weight loss caused by decomposition of MDI-based hard segments in polyurethanes was observed at about 245 °C [43]. The rapid weight loss between 250 °C and 440 °C was associated with decomposition of the soft segments [44]. The 5% weight loss temperatures for all samples are recorded in Table 2,

Table 2
The thermal properties of poly(urethane-urea)s and pure polyether diols measured using DSC and TGA.

Sample code	ρ (g/cm^3)	FFV	T_g (°C)	T_m (°C)	5% weight loss temperature (°C)
I	1.019	0.200	−63.4	N/A	284
II	1.050	0.161	−70.1	12.3	284
III	1.082	0.148	−74.9	4.5	288
IV	1.117	0.151	−81.5/−28.4[a]	10.4	291
V	1.214	0.127[b]	−44.4	37.3	291

[a] Sample IV exhibited two glass transition temperatures because it contains two polyethers.
[b] All FFV values were calculated using the density listed in this table, except for that of sample V. In this case, the estimated amorphous phase density, 1.207 g/cm^3, was used to calculate FFV using Eq. (7). The soft segment and hard segment molar ratios in the amorphous phase were also recalculated for the group contribution method to eliminate the influence of the crystalline region on the calculation of V_0. This calculation assumes that only PEO segments crystallize.

and all TGA curves are presented in Supplementary Information for brevity. These temperatures are similar (284–291 °C) because of the similarity among the chemical structures of the polymers in this study. Moreover, they are consistent with temperatures reported for other poly(urethane-urea) copolymers [36,45].

DSC thermograms of poly(urethane-urea) films are presented in Fig. 2(a), and Table 2 summarizes the thermal transitions from these DSC scans. DSC data were taken during the first heating of the poly(urethane-urea) samples. Fig. 2(b) shows an expanded version of Fig. 2(a) to highlight the glass transition region. The glass transition temperatures of the soft segments are of interest because they are related to microphase separation in such segmented poly(urethane-urea)s; if the microphase separation between hard and soft segments is incomplete, the T_g of the soft segments will often increase beyond the value associated with the T_g of a polymer composed of pure soft segments [46]. The hard segment T_g sometimes cannot be observed because of the relatively weak signal of this glass transition temperature and incomplete microphase separation in the hard segment domains [26].

Sample I (PPG-based) exhibits only a glass transition temperature; all other samples showed both glass transition and melting points. The glass transition temperature of sample I, −63.4 °C, is near the T_g of pure polypropylene glycol (−70 °C) [46] but lower than the reported T_g in crosslinked PPG systems (−43 °C) [47] and PPG containing polyurethanes (−35.7 °C and −39.8 °C) [36]. However, sample I has much higher soft segment content (83.1 wt%) than that of other polyurethanes reported in the literature, which are usually restricted to soft segment contents below 65% [4,26,36,48]. Our DSC measurements showed that the hard and soft segment phases should be well phase-separated in sample I because the thermal transition temperature is quite close to that of pure PPG, reflecting very little mixing of hard and soft segment domains.

Similar behavior was observed in the Terathane®-based poly(urethane-urea)s (i.e., samples II, III, and IV). The melting temperature in samples II and III are 12.3 °C and 4.5 °C, respectively, consistent with the reported melting temperatures of the Terathane® phase in Terathane®-based polyurethanes [48,49]. The reported glass transition temperatures of Terathane® soft segments, however, varies from −38.7 °C to −80.8 °C [2,48–50], depending on the polyether molecular weight, hard segment content, and the nature and amount of any additional polyether components in polyurethanes and poly(urethane-urea)s. Based on our DSC experiments, the glass transition temperatures of II and III are −71.8 °C and −70.1 °C, respectively, close to the values (−75 °C and −76.2 °C) for polyurethanes containing 74.2 wt% soft segment with a polyether molecular weight of 2400 and 2030, reported by Galland and Lam [48].

In sample IV, two glass transition temperatures were observed at −78.9 °C (Terathane®) and −28.4 °C (PEG) showing that the soft segments were phase separated. A very weak transition was also observed between 10 and 15 °C that may due to low levels of crystallinity in one of the soft segment phases. However, the enthalpy (less than 1 J/g) is much smaller than that of either Terathane®-based (around 20 J/g) or PEG-based (51 J/g) poly(urethane-urea)s, and there was no observation of a melting transition of the other soft segment phase, showing that mixing the two polyethers disrupts crystallinity in the final product. Such a situation is desirable for preparing highly permeable polymers, since crystallinity reduces gas permeability [10]. Similar results were reported by Jiang et al. [44] in polyurethanes containing PEG/PDMS soft segment mixtures.

As Fig. 2(a) shows, sample V is the only polymer having a semi-crystalline structure above room temperature. DSC analysis showed that the melting point is 37 °C, slightly lower than the melting temperature of the pure PEG 2000 starting material, which was 51 °C based on DSC analysis. In semi-crystalline polymers, gas molecules are presumed to permeate only through amorphous regions [51]. Thus, it is of interest to determine the crystallinity in any sample, such as sample V, which may have some crystallinity at the temperature of gas permeation studies. Even though there are potentially urethane/urea linkages from the hard segments dissolving in the soft segment region, we presume that the crystalline phase contains only polyether structures because of the well-organized packing of molecules in crystals. Moreover, WAXD data, to be discussed below, support the assignment of the crystalline region to be composed of PEG crystals. Therefore, the weight fraction crystallinity in the crystals, χ_C (g crystals/g soft segment material), was estimated as follows [52]:

$$\chi_C = \frac{\Delta H}{\Delta H_C} \tag{5}$$

where ΔH is the melting enthalpy obtained from the DSC melting peak area, and ΔH_C is the melting enthalpy of 100% crystalline polyethylene oxide. The weight fraction of crystallinity in the entire poly(urethane-urea), χ'_C (g crystals/g polymer), can be estimated based on the soft segment content listed in Table 2 and χ_C in the soft segments. The ΔH_C value used for PEG in this calculation, 166.4 J/g, was suggested by Simon and Rutherford [53]. From DSC analysis, the ΔH value of sample V was 56.1 J/g. Using this value in Eq. (5) yields a crystallinity of 33.7 wt% in the PEG soft segments and 26.4 wt% crystallinity in sample V.

Volume fraction crystallinity, ϕ_C, can be calculated as follows [54]:

$$\phi_C = \left(\frac{\rho}{\rho_c}\right)\chi'_C \tag{6}$$

or [51]:

$$\phi_C = \frac{\rho - \rho_a}{\rho_c - \rho_a} \tag{7}$$

where ρ is the measured poly(urethane-urea) density, ρ_c is the density of crystalline PEO at room temperature (1.234 g/cm^3 [53]), and ρ_a is the density of amorphous regions in the poly(urethane-urea) sample. The film density of sample V, according to Table 2, is 1.214 g/cm^3. Using this value in Eq. (6) yields a volume frac-

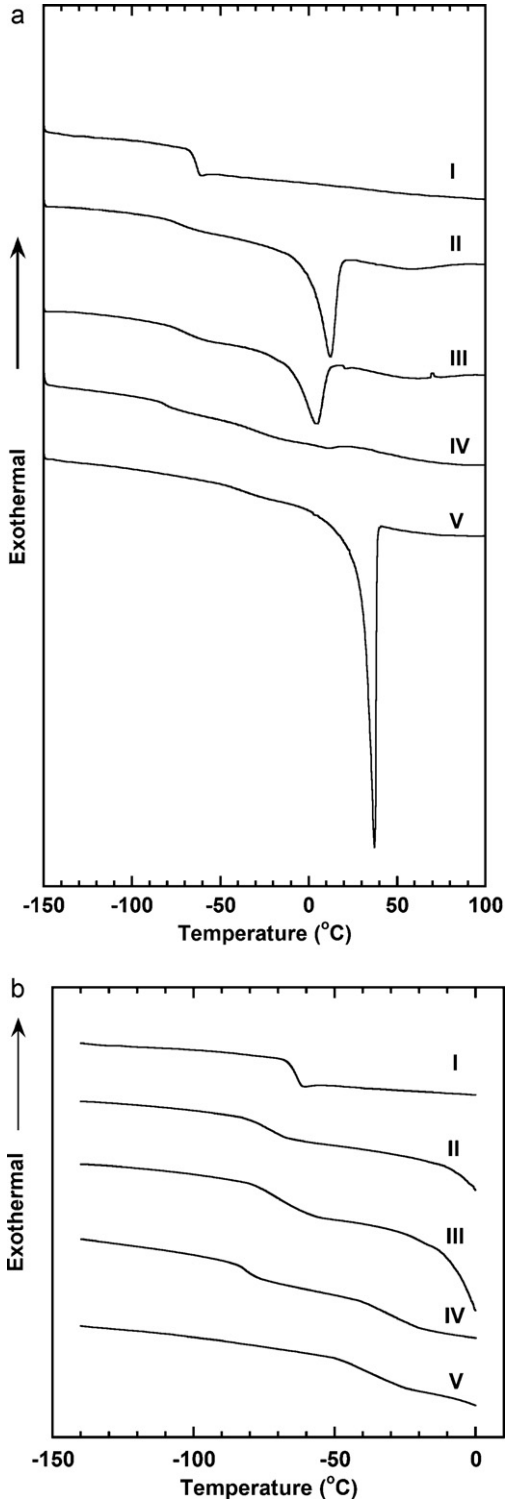

Fig. 2. Differential scanning calorimetry (DSC) thermograms of (a) glass transition and melting, and (b) only glass transition of poly(urethane-urea) samples prepared using solution casting. The heating rate was 10 °C/min. The thermograms have been displaced vertically for clarity. The thermograms have been displaced vertically for easier viewing.

tion crystallinity of 26.0%. From this calculation, one may estimate the density of the amorphous regions of this sample, ρ_a, to be 1.207 g/cm^3 based on Eq. (7). This value will be used to calculate fractional free volume in the amorphous regions of this sample.

WAXD was also conducted to characterize the morphology in these samples. Fig. 3 presents the X-ray diffraction spectra of

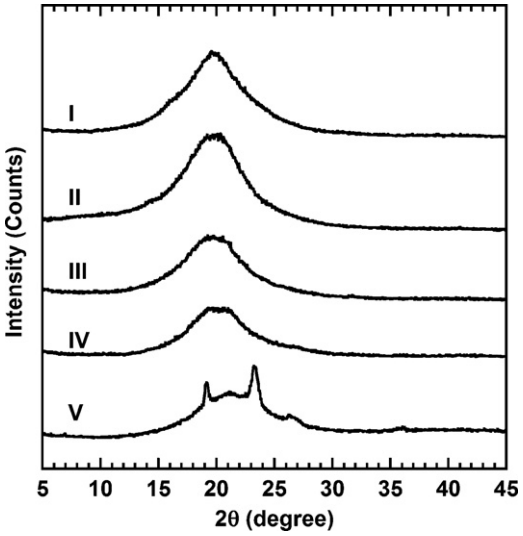

Fig. 3. WAXD analyses of poly(urethane-urea) films. The curves have been displaced vertically for clarity.

these poly(urethane-urea)s. The reflection peak ascribed to the amorphous regions of the samples was observed at 2θ values of approximately 19.5°, which is similar to reported values in other poly(urethane-urea)s [55]. Except for sample V, all other samples showed only an amorphous halo. In sample V, two sharp peaks appear at $2\theta = 19.2°$ and $2\theta = 23.3°$, respectively, which are ascribed to crystalline PEO structures in the polymer [56]. The weight fraction of the crystalline region in this sample was estimated from the WAXD data as follows [54]:

$$\chi_C' = \frac{I_C}{I_C + I_A} \tag{8}$$

where I_A and I_C were the integrated areas under the amorphous and crystalline peaks, respectively. Based on Eq. (5) and the WAXD pattern, the crystalline weight fraction of sample V would be 22%. The weight fraction and volume fraction crystallinity values obtained from DSC and WAXD analysis appear in Table 3. Typically, the amount of crystallinity estimated from DSC and WAXD will not agree perfectly, because different assumptions are used to determine crystallinity values from these different techniques [54,57]. For example, Eq. (8) is based on the assumption that all polymer chains in the crystalline region contribute to I_C, and only chains in the amorphous region contribute to I_A. However, the estimated crystallinity values based on the WAXD measurements are sometimes lower than the crystallinity estimated using other methods such as DSC and density. Such lower crystallinity values are ascribed to the existence of a transition region between the crystalline and amorphous regions [58], or defects in crystalline regions [59]. Therefore, we used the DSC crystallinity value in the amorphous phase density and FFV calculation. However, the WAXD data are in reasonable agreement with the crystallinity values from DSC.

3.2. Density and FFV

The amount of free volume in the polymer matrix is an important parameter influencing gas transport properties [60]. Fractional

Table 3
Volume and weight percent crystallinity in sample V (PEG 2000 based).

Technique for estimating crystallinity	χ'_C (%)	ϕ_C (%)
DSC	26	26
WAXD	22	22

ϕ_C values were estimated from χ_C values using Eq. (6).

free volume can be estimated as follows [61]:

$$\mathrm{FFV} = \frac{V_{sp} - V_0}{V_{sp}} \approx \frac{V_{sp} - 1.3V_w}{V_{sp}} \quad (9)$$

where V_{sp} is the polymer specific volume at the temperature of interest, V_0 is the occupied volume of polymer at 0 K, which is estimated as 1.3 times the van der Waals volume (V_w) calculated by group contribution methods [62,63]. With the exception of sample V, the poly(urethane-urea)s presented in this work are totally amorphous at or above room temperature. The densities of these materials at ambient conditions are presented in Table 2. Table 2 also provides the fractional free volumes of these samples, calculated as described above. For the case of sample V, which is semi-crystalline at ambient conditions, the estimated amorphous phase density was used in the FFV calculation. Based on the amorphous polymer density and estimated van der Waals volume, sample I has the highest FFV (0.200), which may be due to the extra–CH_3 groups along the main chain of the soft segments. Interestingly, this FFV value is near the FFV (around 0.190) in crosslinked PPG materials [47]. In samples II and III, an increase in Terathane® molecular weight (from 2000 to 2900) increases the soft segment content and, consequently, increases FFV from 0.148 to 0.161. For the FFV of sample IV, a 50/50 ratio of Terathane® and PEG was used to calculate V_w values for the soft segments, and the FFV is similar to that of sample III. The FFV in sample V, however, cannot be simply calculated using the film density and van der Waals volume obtained from the group distribution method based on the total polymer composition. Since part of the PEG chains are sequestered in crystals, the chemical composition of the amorphous phase must be recalculated to account for this fact. Based on the χ_C value estimated from DSC analysis (as shown in Table 3), the mole ratio of soft to hard segments in the amorphous phase is 1.46:1, and the FFV in the amorphous phase is 0.127, which is lower than that of the other poly(urethane-urea)s in this work.

3.3. Water uptake

Water uptake values for poly(urethane-urea) samples are also reported in Table 1. The sample synthesized from PEG 2000 (sample V) has around 130 wt% water uptake, while the water uptake is only about 35 wt% for sample IV, which contains 50% PEG 2000 and 50% Terathane® 2000 soft segments. For comparison, in crosslinked amorphous PEG systems, the water uptake can vary from 110% to about 350%, depending on the preparation conditions [64]. Clearly, water uptake depends strongly on the polyethylene oxide content. A more detailed study of this phenomenon is provided elsewhere [65,66]. Although PPG and Terathane® have similar ether structures in the polymer main chain, the water uptakes for these polymers are much lower. Sample I (PPG-based) has only 17 wt% water uptake, and samples II and III (Terathane®-based) are only around 10 wt%. The water uptake data illustrate that PPG and Terathane® containing materials are much less hydrophilic than those based on PEO and should, therefore, be much less sensitive to humidity.

3.4. Gas transport properties

Fig. 4 presents the pure gas permeability coefficients of N_2, and CO_2 in poly(urethane-urea) membranes at 35 °C as a function of upstream pressure. The permeability coefficients of O_2, H_2, He and CH_4 were also measured, and the detailed data for these gases are presented in Supplementary Information for brevity. The permeability coefficient change *vs.* upstream pressure is similar to that in rubbery polymers [67]. That is, the permeability coefficients of permanent gases, such as N_2, O_2, H_2, CH_4 and He, are essentially independent of upstream pressure, and the permeability of CO_2 increases somewhat with increasing upstream pressure.

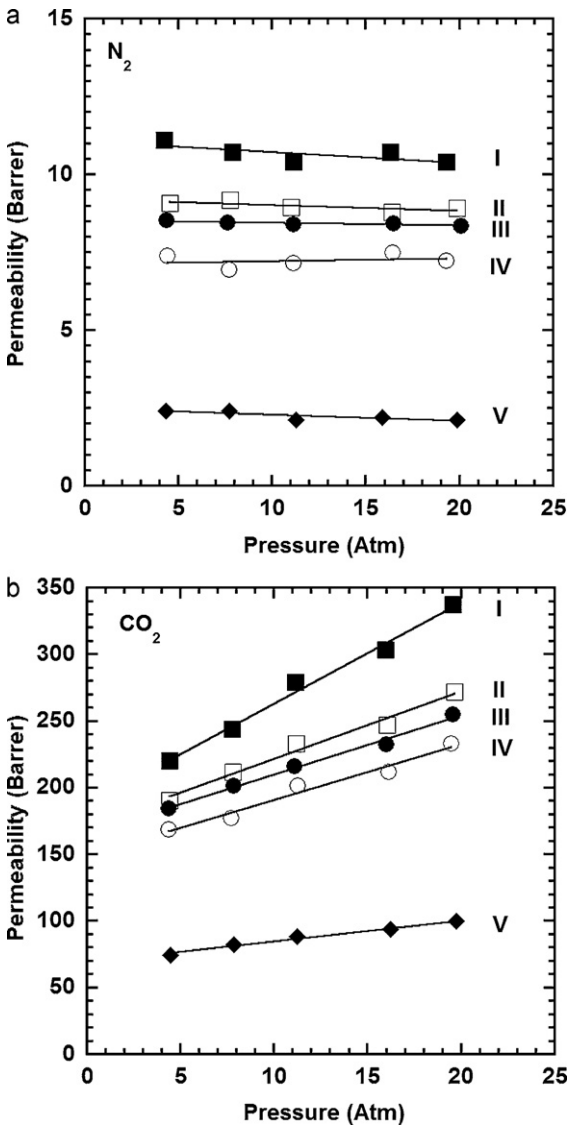

Fig. 4. Pure gas permeability of: (a) N_2 and (b) CO_2 in polymer films prepared from samples I (■), II (□), III (●), IV (○) and V (♦) as a function of upstream pressure at 35 °C.

This effect is normally observed in rubbery polymers often because the presence of strong sorbing penetrants (such as CO_2) can plasticize the polymer matrix and increase polymer local segmental motion, resulting in an increase in diffusivity [17,67]. With increasing pressure, both CO_2 solubility and diffusivity can increase as CO_2 concentration in the polymer increases. Both of these effects lead to an increase in CO_2 gas permeability. The relationship between permeability and upstream pressure can be described by the following empirical model [68]:

$$P_A = P_{A,0}(1 + m\,\Delta p) = P_{A,0}(1 + mp_2) \quad (10)$$

where P_A is the permeability coefficient at an upstream pressure, p_2; $P_{A,0}$ is the permeability coefficient at $p_2 = 0$ (i.e., infinite dilution); m is an adjustable constant; and Δp is the pressure difference between the upstream and downstream faces of the film, $\Delta p = p_2 - p_1$. In this study, the downstream pressure was much lower than the upstream pressure, so the downstream pressure can be neglected, and Δp can be replaced by p_2. Infinite dilution permeability coefficients for different gases in these poly(urethane-urea) block copolymers were calculated using Eq. (10), and the results are recorded in Table 4.

Table 4
Pure gas permeability in poly(urethane-urea) films at 35 °C and infinite dilution.

Polymer	$P_{A,0}$ (Barrer)						Permeability selectivity				
	O_2	N_2	H_2	He	CH_4	CO_2	CO_2/H_2	CO_2/N_2	CO_2/O_2	CO_2/CH_4	O_2/N_2
I	28	11	42	41	34	190	4.5	17	6.8	5.5	2.5
II	22	9.2	37	35	25	170	4.6	19	7.7	6.7	2.4
III	21	8.5	35	28	20	170	4.8	20	7.8	7.9	2.5
IV	20	7.2	32	25	22	150	4.3	21	7.6	6.9	2.7
V	8.0	2.4	12	10	9.1	69	5.8	29	8.6	7.6	3.3

Gas permeability increases as FFV increases. For example, sample I has the highest FFV (0.200), and it also has the highest infinite dilution permeability to all gases. Sample II has higher permeability than sample III. The higher soft chain molecular weight increases soft segment content, enhances FFV and leads to increased permeability [48]. Sample V has lower gas permeability than all other materials, perhaps due to the semi-crystalline structure in the PEG soft segments and low FFV in the amorphous phase. The permeability measurements were conducted at 35 °C, which is in the window where some of the PEG crystals melt. Based on the fraction of the area under the DSC melting curve at temperatures up to 35 °C, it appears that about 40% of the crystals would have melted when the temperature was raised from ambient to 35 °C, so approximately 60% of the crystalline material (i.e., approximately 16 wt% of the polymer) would remain during the permeation measurement. So the crystallinity at the conditions of the permeability measurements was around 13% by volume of the PEG soft segments and 10–11% by volume based in the polymer. PEG 2000-based sample V has permeability coefficients similar to those of amorphous crosslinked PEO [13] but larger than those of semi-crystalline PEO [51]. For example, the nitrogen permeability coefficients (35 °C) in sample V, crosslinked PEO and semi-crystalline PEO were 2.4 Barrer, 2.1 Barrer, and 0.24 Barrer, respectively. This divergence may be due to the great differences in the extent of crystallinity (71 vol. % in semi-crystalline PEO, but only 10–11 vol. % in sample V). Compared to sample V, sample IV only contains 50 wt% PEG 2000 in the soft segments, and replacing the other 50% of the polyether with Terathane® 2000 results in a more amorphous structure at room temperature and higher FFV in the amorphous phase, as shown in Fig. 3 and Table 2. This change in the soft segment composition leads to a significant increase, by more than a factor of two, in permeability. For example, the N_2 infinite dilution permeability increases from 2.4 Barrer in sample V to 7.2 Barrer in sample IV, while the CO_2 infinite dilution permeability increases from 69 Barrer to 150 Barrer.

The permeability coefficients decrease in the following order:

$$CO_2 > H_2 > He > CH_4 \approx O_2 > N_2.$$

Except for hydrogen and helium, the order of the permeability coefficients reflects the order of decreasing gas critical temperature, which is often associated with a decrease in gas solubility in polymers [67]. That is, penetrants with higher critical temperature are usually more condensable and have higher solubility coefficients. Thus, in poly(urethane-urea)s based on polyether diols, CO_2 is often more permeable than smaller penetrants, such as H_2, because the much higher CO_2 solubility (relative to that of H_2) more than offsets the somewhat lower diffusion coefficient of CO_2. H_2 and He, which would be expected to have low solubility but are the smallest gases considered, so they should have high diffusion coefficients, were more permeable than all other gases except CO_2 [51]. This order of permeability coefficients reflects the competing effects of solubility, which favors more condensable (and often larger) penetrants, and diffusivity, which favors smaller (and often less soluble) gases, on permeability.

The permeability selectivities for different gas pairs are also shown in Table 4. Sample I has the highest gas permeability but low selectivity values. Samples II and III have permeabilities close to those of sample I but better gas separation properties than those of sample I. Sample V has the best O_2/N_2 permeability selectivity as well as the highest CO_2 separation properties from other gases. However, it has the lowest permeability coefficients. This result may be due to some residual crystallinity in the sample during the permeation measurements as well as the higher hard segment content in the amorphous phase. The hard segment content is related to the morphology and microphase-separation in the soft segment regions [26,69]. In this regard, the rigid urethane/urea linkages are reported to act as fillers or physical crosslinks in polyurethanes [70]. Various studies [5,48,70,71] have reported that increasing hard segment content (i.e., decreasing soft segment content) reduces permeability and *vice versa*.

The lower overall CO_2 permeability selectivity in PPG and Terathane®-based poly(urethane-urea)s is somewhat balanced by higher CO_2 permeability, as shown in Fig. 5. Sample I, which has lower CO_2 selectivity over other gases, maintains higher CO_2 permeability relative to the other poly(urethane-urea)s. Since low FFV usually leads to a decrease in gas permeability but an increase in diffusivity selectivity [72], there is often a trade-off between permeability and selectivity [73,74]. In rubbery polymers containing PEO or PPO linkages, the change in FFV does not strongly decrease CO_2 permeability selectivity, as it would in glassy polymers, because the diffusion coefficient is not strongly affected by penetrant molecular size, and the permeability selectivity is strongly influenced by differences in solubility selectivity [17,47]. As shown in Fig. 5, only CO_2/N_2 selectivity showed a decrease with increasing CO_2 permeability; CO_2 separation properties over other gases are less strongly affected than is the infinite dilution

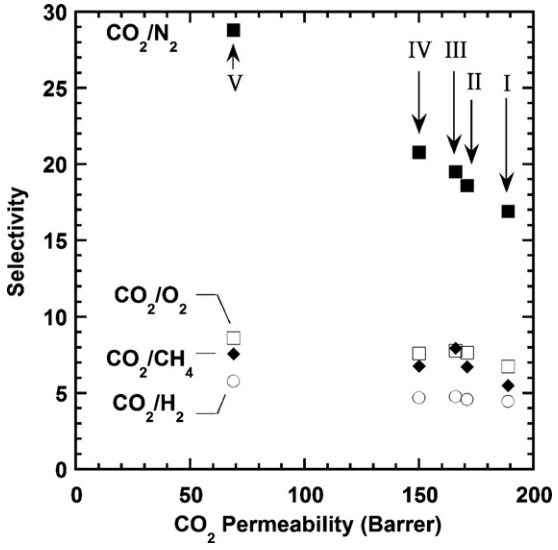

Fig. 5. Pure gas selectivities of CO_2/N_2 (■), CO_2/O_2 (●), CO_2/CH_4 (♦), and CO_2/H_2 (○) in poly(urethane-urea) membranes as a function of CO_2 permeability at 35 °C.

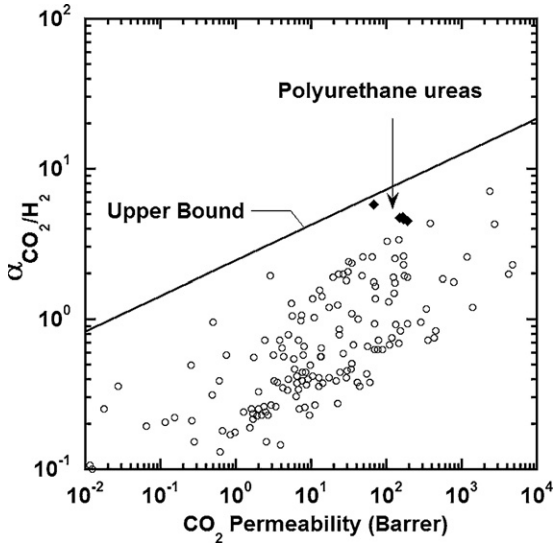

Fig. 6. Comparison of CO_2/H_2 selectivity *vs.* CO_2 permeability of poly(urethane-urea)s prepared in the present study (♦) with other polymers (○) from the literature [13]. Data at lower CO_2 permeability values correspond to lower CO_2 partial pressures in the feed gas and *vice versa*. The upper bound from the literature [13] was drawn based on a model prediction [73].

CO_2 permeability. The CO_2/H_2 selectivity values are presented as a function of CO_2 permeability in Fig. 6 along with reported values from other polymer materials [73]. Unlike cases where the separation is based on strong size-sieving ability, the positive slope of the upper bound indicates that high CO_2 permeability and high CO_2/H_2 selectivity may be achieved simultaneously. The slightly higher CO_2/H_2 permeability selectivity of sample I, as shown in Fig. 6 may be attributed to the better solubility of CO_2 in PEG than in PPG and Terathane® polymers [25]. The CO_2/H_2 selectivity values in Fig. 6 show that the materials have interesting CO_2/H_2 separation properties. It has been reported that polymers prepared using different polyether structures and different preparation protocols also have similar or higher CO_2 permeability, as well as CO_2/H_2 and CO_2/N_2 selectivity. Our results are consistent with previous studies indicating the strong, positive effect of ethylene oxide units, in particular, for increasing CO_2 permeability and CO_2/H_2 and CO_2/N_2 separation properties. As discussed previously, the CO_2 permeability and permeability selectivity are affected not only by the soft and hard segment chemical structures and contents, but also by the phase separation extent between hard and soft segments in such materials.

4. Conclusions

The physical and gas transport properties of a systematic series of poly(urethane-urea)s were determined. The presence of different polyether diols affects thermal transitions as well as the fractional free volume and leads to changes in gas transport performance. Samples synthesized from PEG 2000 have a semi-crystalline structure at room temperature. The crystallization reduces soft segment content in the amorphous phase and leads to lower permeability. However, replacing half of the PEG soft segments with Terathane® results in an essentially amorphous material and increases gas permeability approximately threefold. PPG-based poly(urethane-urea) has the highest FFV, as well as the highest permeability, but the CO_2 selectivity over other gases decreases slightly. The Terathane®-based polymers also have good gas permeability and better CO_2 separation properties than PPG-based materials. Both PPG- and Terathane®-based polymers exhibit much lower water uptake than PEG base materials (about 150 wt% in PEG-based, 17 wt% in PPG-based and 10 wt% in Terathane®-based polymer), showing that in an environment with high humidity, these materials may achieve more stable separation properties than those of materials based on PEG.

Acknowledgements

This research is based upon work supported in part by the National Science Foundation under Grant No. DMR #0423914 and by the Department of Energy under Grant No. DE-FG02-02ER15362. The authors also gratefully acknowledge support provided by Air Liquide-MEDAL™ (Newport, DE). The authors also offer their sincere thanks to Dr. Steve Swinnea at the University of Texas at Austin for his help with the WAXD analysis.

Appendix A. Supplementary data

Supplementary data associated with this article can be found, in the online version, at doi:10.1016/j.memsci.2010.11.024.

References

[1] D. Dieterich, E. Grigat, W. Hahn, H. Hespe, H.G. Schmelzer, Principles of polyurethane chemistry and special applications, in: G. Oertel (Ed.), Polyurethane Handbook: Chemistry, Raw Materials, Processing, Application, Properties, Hanser Gardner Publication, Cincinnati, OH, 1994, pp. 11–31.
[2] S. Abouzahr, G.L. Wilkes, Structure property studies of polyester- and polyether-based MDI-BD segmented polyurethanes: effect of one- vs. 2-stage polymerization conditions, Journal of Applied Polymer Science 29 (9) (1984) 2695–2711.
[3] M. Pegoraro, L. Zanderighi, A. Penati, F. Severini, F. Bianchi, N. Cao, R. Sisto, C. Valentini, Polyurethane membranes from polyether and polyester diols for gas fractionation, Journal of Applied Polymer Science 43 (4) (1991) 687–697.
[4] L.S. Teo, J.F. Kuo, C.Y. Chen, Study on the morphology and permeation property of amine group-contained polyurethanes, Polymer 39 (15) (1998) 3355–3364.
[5] P.M. Knight, D.J. Lyman, Gas permeability of various block copolyether urethanes, Journal of Membrane Science 17 (3) (1984) 245–254.
[6] M. Yoshino, K. Ito, H. Kita, K.-I. Okamoto, Effect of hard-segment polymers on CO_2/N_2 gas-separation properties of poly(ethylene oxide)-segmented copolymers, Journal of Polymer Science Part B: Polymer Physics 38 (2000) 1707–1715.
[7] M.B. Shiflett, H.C. Foley, Ultrasonic deposition of high-selectivity nanoporous carbon membranes, Science 285 (5435) (1999) 1902–1905.
[8] J.M.S. Henis, M.K. Tripodi, The developing technology of gas separating membranes, Science 220 (4592) (1983) 11–17.
[9] R.W. Baker, J.G. Wijmans, J.H. Kaschemekat, The design of membrane vapor–gas separation systems, Journal of Membrane Science 151 (1) (1998) 55–62.
[10] H.Q. Lin, B.D. Freeman, Materials selection guidelines for membranes that remove CO_2 from gas mixtures, Journal of Molecular Structure 739 (1–3) (2005) 57–74.
[11] W.J. Koros, Barrier polymers and structures: overview, in: W.J. Koros (Ed.), Barrier Polymers and Structures:, American Chemical Society, Washington, DC, 1990, pp. 1–22.
[12] S. Matteucci, Y. Yampolskii, B.D. Freeman, I. Pinnau, Transport of gases and vapors in glassy and rubbery polymers, in: Y. Yampolskii, B.D. Freeman, I. Pinnau (Eds.), Material Science of Membranes for Gas and Vapor Separation, John Wiley & Sons, New York, 2006, pp. 1–47.
[13] H.Q. Lin, E. Van Wagner, B.D. Freeman, L.G. Toy, R.P. Gupta, Plasticization-enhanced hydrogen purification using polymeric membranes, Science 311 (5761) (2006) 639–642.
[14] H. Lin, B.D. Freeman, Gas and vapor solubility in cross-linked poly(ethylene glycol diacrylate), Macromolecules 38 (20) (2005) 8394–8407.
[15] S. Kelman, H.Q. Lin, E.S. Sanders, B.D. Freeman, CO_2/C_2H_6 separation using solubility selective membranes, Journal of Membrane Science 305 (1–2) (2007) 57–68.
[16] H.Q. Lin, T. Kai, B.D. Freeman, S. Kalakkunnath, D.S. Kalika, The effect of cross-linking on gas permeability in cross-linked poly(ethylene glycol diacrylate), Macromolecules 38 (20) (2005) 8381–8393.
[17] H.Q. Lin, E. Van Wagner, J.S. Swinnea, B.D. Freeman, S.J. Pas, A.J. Hill, S. Kalakkunnath, D.S. Kalika, Transport and structural characteristics of crosslinked poly(ethylene oxide) rubbers, Journal of Membrane Science 276 (1–2) (2006) 145–161.
[18] H. Lin, E. Van Wagner, R. Raharjo, B.D. Freeman, I. Roman, High-performance polymer membranes for natural-gas sweetening, Advanced Materials 18 (1) (2006) 39–44.
[19] V.I. Bondar, B.D. Freeman, I. Pinnau, Gas sorption and characterization of poly(ether-b-amide) segmented block copolymers, Journal of Polymer Science Part B: Polymer Physics 37 (17) (1999) 2463–2475.
[20] V.I. Bondar, B.D. Freeman, I. Pinnau, Gas transport properties of poly(ether-b-amide) segmented block copolymers, Journal of Polymer Science Part B: Polymer Physics 38 (15) (2000) 2051–2062.

[21] J.H. Kim, Y.M. Lee, Gas permeation properties of poly(amide-6-b-ethylene oxide)-silica hybrid membranes, Journal of Membrane Science 193 (2) (2001) 209–225.
[22] V. Barbi, S.S. Funari, R. Gehrke, N. Scharnagl, N. Stribeck, SAXS and the gas transport in polyether-block-polyamide copolymer membranes, Macromolecules 36 (3) (2003) 749–758.
[23] S.J. Metz, M.H.V. Mulder, M. Wessling, Gas-permeation properties of poly(ethylene oxide) poly(butylene terephthalate) block copolymers, Macromolecules 37 (12) (2004) 4590–4597.
[24] W. Yave, A. Car, S.S. Funari, S.P. Nunes, K.V. Peinemann, CO_2-philic polymer membrane with extremely high separation performance, Macromolecules 43 (1) (2010) 326–333.
[25] K. Okamoto, M. Fujii, S. Okamyo, H. Suzuki, K. Tanaka, H. Kita, Gas permeation properties of poly(ether imide) segmented copolymers, Macromolecules 28 (20) (1995) 6950–6956.
[26] M. Yoshino, K. Ito, H. Kita, K.I. Okamoto, Effects of hard-segment polymers on CO_2/N_2 gas separation properties of poly(ethylene oxide) segmented copolymers, Journal of Polymer Science Part B: Polymer Physics 38 (13) (2000) 1707–1715.
[27] A. Car, C. Stropnik, W. Yave, K.V. Peinemann, Pebax (R)/polyethylene glycol blend thin film composite membranes for CO_2 separation: performance with mixed gases, Separation and Purification Technology 62 (1) (2008) 110–117.
[28] ASTM D4274-05, Standard Test Methods for Testing Polyurethane Raw Materials: Determination of Hydroxyl Numbers of Polyols, 2001.
[29] ASTM D5155-07, Standard Test Methods for Polyurethane Raw Materials: Determination of the Isocyanate Content of Aromatic Isocyanates, 2007.
[30] A. Car, C. Stropnik, W. Yave, K.V. Peinemann, Tailor-made polymeric membranes based on segmented block copolymers for CO_2 separation, Advanced Functional Materials 18 (18) (2008) 2815–2823.
[31] P. Zoller, D. Walsh, Standard Pressure–Volume–Temperature Data for Polymers, 1st ed., Technomic Publishing Company, Inc., Lancaster, 1995.
[32] A. Car, C. Stropnik, W. Yave, K.V. Peinemann, PEG modified poly(amide-b-ethylene oxide) membranes for CO_2 separation, Journal of Membrane Science 307 (1) (2008) 88–95.
[33] H. Yasuda, C.E. Lamaze, L.D. Ikenberry, Permeability of solutes through hydrated polymer membranes. I. Diffusion of sodium chloride, Die Makromolekulare Chemie 118 (1) (1968) 19–35.
[34] K. Nagai, S. Tanaka, Y. Hirata, T. Nakagawa, M.E. Arnoldb, B.D. Freeman, D. Lerouxc, D.E. Bettsc, J.M. DeSimonec, F.A. DiGiano, Solubility and diffusivity of sodium chloride in phase-separated block copolymers of poly(2-dimethylaminoethyl methacrylate), poly(1,1′-dihydroperfluorooctyl methacrylate) and poly(1,1,2,2-tetrahydroperfluorooctyl acrylate), Polymer 42 (25) (2001) 9941–9948.
[35] T.O. Ahn, I.S. Choi, H.M. Jeong, K. Cho, Thermal and mechanical properties of thermoplastic polyurethane elastomers from different polymerization methods, Polymer International 31 (1993) 329–333.
[36] H.B. Park, C.K. Kim, Y.M. Lee, Gas separation properties of polysiloxane/polyether mixed soft segment urethane urea membranes, Journal of Membrane Science 204 (1–2) (2002) 257–269.
[37] J.M. Orban, T.M. Chapman, W.R. Wagner, R. Jankowski, Easily grafted polyurethanes with reactive main chain functional groups. Synthesis, characterization, and antithrombogenicity of poly(ethylene glycol)-grafted poly(urethanes), Journal of Polymer Science Part A: Polymer Chemistry 37 (17) (1999) 3441–3448.
[38] T. Tawa, S. Ito, Preparation and reactions of hydrophilic isocyanate micelles dispersed in water, Colloid and Polymer Science 283 (7) (2005) 731–737.
[39] F.M.B. Coutinho, M.C. Delpech, Degradation profile of films cast from aqueous polyurethane dispersions, Polymer Degradation and Stability 70 (1) (2000) 49–57.
[40] L.S. Teo, C.Y. Chen, J.F. Kuo, Fourier transform infrared spectroscopy study on effects of temperature on hydrogen bonding in amine-containing polyurethanes and poly(urethane-urea)s, Macromolecules 30 (6) (1997) 1793–1799.
[41] E. Yilgor, E. Burgaz, E. Yurtsever, I. Yilgor, Comparison of hydrogen bonding in polydimethylsiloxane and polyether based urethane and urea copolymers, Polymer 41 (3) (2000) 849–857.
[42] Y.M. Song, W.C. Chen, T.L. Yu, K. Linliu, Y.H. Tseng, Effect of isocyanates on the crystallinity and thermal stability of polyurethanes, Journal of Applied Polymer Science 62 (5) (1996) 827–834.
[43] Y.T. Shieh, H.T. Chen, K.H. Liu, Y.K. Twu, Thermal degradation of MDI-based segmented polyurethanes, Journal of Polymer Science Part A: Polymer Chemistry 37 (22) (1999) 4126–4134.
[44] X. Jiang, J.F. Ding, A. Kumar, Polyurethane–poly(vinylidene fluoride) (PU–PVDF) thin film composite membranes for gas separation, Journal of Membrane Science 323 (2) (2008) 371–378.
[45] R.A. Azzam, S.K. Mohamed, R. Tol, V. Everaert, H. Reynaers, B. Goderis, Synthesis and thermo-mechanical characterization of high performance polyurethane elastomers based on heterocyclic and aromatic diamine chain extenders, Polymer Degradation and Stability 92 (7) (2007) 1316–1325.
[46] J.P. Santerre, J.L. Brash, Microstructure of polyurethane ionomers derivatized with dodecylamine and polyethylene oxide in the hard segment, Journal of Applied Polymer Science 52 (4) (1994) 515–523.
[47] R.D. Raharjo, H.Q. Lin, D.E. Sanders, B.D. Freeman, S. Kalakkunnath, D.S. Kalika, Relation between network structure and gas transport in crosslinked poly(propylene glycol diacrylate), Journal of Membrane Science 283 (1–2) (2006) 253–265.
[48] G. Galland, T.M. Lam, Permeability and diffusion of gases in segmented polyurethanes: structure–properties relations, Journal of Applied Polymer Science 50 (6) (1993) 1041–1058.
[49] B.C. Chun, T.K. Cho, M.H. Chong, Y.C. Chung, Structure–property relationship of shape memory polyurethane cross-linked by a polyethyleneglycol spacer between polyurethane chains, Journal of Materials Science 42 (21) (2007) 9045–9056.
[50] S. Abouzahr, G.L. Wilkes, Z. Ophir, Structure property behavior of segmented polyether MDI butanediol based urethanes: effect of composition ratio, Polymer 23 (7) (1982) 1077–1086.
[51] H. Lin, B.D. Freeman, Gas solubility, diffusivity and permeability in poly(ethylene oxide), Journal of Membrane Science 239 (2004) 105–117.
[52] S. Sunderrajan, B.D. Freeman, C.K. Hall, I. Pinnau, Propane and propylene sorption in solid polymer electrolytes based on poly(ethylene oxide), Journal of Membrane Science 182 (1–2) (2001) 1–12.
[53] F.T. Simon, J.M. Rutherford, Crystallization and melting behavior of polyethylene oxide copolymers, Journal of Applied Physics 35 (82) (1964) 82–86.
[54] S.N. Dhoot, B.D. Freeman, M.E. Stewart, Sorption and transport of linear alkane hydrocarbons in biaxially oriented polyethylene terephthalate, Journal of Polymer Science Part B: Polymer Physics 39 (11) (2001) 1160–1172.
[55] T. Takahashi, N. Hayashi, S. Hayashi, Structure and properties of shape-memory polyurethane block copolymers, Journal of Applied Polymer Science 60 (7) (1996) 1061–1069.
[56] N. Ravi, A. Mitra, P. Hamilton, F. Horkay, Characterization of the network properties of poly(ethylene glycol)-acrylate hydrogels prepared by variations in the ethanol–water solvent composition during crosslinking copolymerization, Journal of Polymer Science Part B: Polymer Physics 40 (23) (2002) 2677–2684.
[57] C.C. McDowell, B.D. Freeman, G.W. McNeely, Acetone sorption and uptake kinetic in poly(ethylene terephthalate), Polymer 40 (12) (1999) 3487–3499.
[58] E.W. Fischer, S. Fakirov, Structure and properties of polyethyleneterephthalate crystallized by annealing in the highly oriented state, Journal of Materials Science 11 (6) (1976) 1041–1064.
[59] L.E. Alexander, X-ray Diffraction Methods in Polymer Science, 2nd ed., R. K. Publishing Company, Malabar, FL, 1985.
[60] B.D. Freeman, I. Pinnau, Polymeric materials for gas separations, in: B.D. Freeman, I. Pinnau (Eds.), Polymer Membranes for Gas and Vapor Separation, vol. 733, ACS Symposium Series, Washington, DC, 1999, pp. 1–27.
[61] M.R. Pixton, D.R. Paul, Relationship between structure and transport properties for polymers with aromatic backbones, in: D.R. Paul, Y.P. Yampol'skii (Eds.), Polymeric Gas Separation Membranes, CRC Press, Boca Raton, 1994, pp. 83–154.
[62] A. Bondi, Physical Properties of Molecular Crystals, Liquid, and Glasses, John Wiley and Sons, New York, 1968.
[63] D.W. van Krevelen, Properties of Polymers: Their Correlation with Chemical Structure; Their Numerical Estimation and Prediction from Additive Group Contributions, Elsevier Science, Amsterdam, 1990.
[64] H. Ju, B.D. McCloskey, A.C. Sagle, Y.H. Wu, V.A. Kusuma, B.D. Freeman, Crosslinked poly(ethylene oxide) fouling resistant coating materials for oil/water separation, Journal of Membrane Science 307 (2) (2008) 260–267.
[65] H. Kitano, K. Ichikawa, M. Ide, M. Fukuda, W. Mizuno, Fourier transform infrared study on the state of water sorbed to poly(ethylene glycol) films, Langmuir 17 (6) (2001) 1889–1895.
[66] S. Lusse, K. Arnold, The interaction of poly(ethylene glycol) with water studied by H-1 and H-2 NMR relaxation time measurements, Macromolecules 29 (12) (1996) 4251–4257.
[67] T.C. Merkel, V.I. Bondar, K. Nagai, B.D. Freeman, I. Pinnau, Gas sorption, diffusion, and permeation in poly(dimethylsiloxane), Journal of Polymer Science Part B: Polymer Physics 38 (2000) 415–434.
[68] A. Singh, B.D. Freeman, I. Pinnau, Pure and mixed gas acetone/nitrogen permeation properties of polydimethylsiloxane [PDMS], Journal of Polymer Science Part B: Polymer Physics 36 (1998) 230–289.
[69] K. Madhavan, B.S.R. Reddy, Poly(dimethylsiloxane-urethane) membranes: effect of hard segment in urethane on gas transport properties, Journal of Membrane Science 283 (1–2) (2006) 357–365.
[70] H. Xiao, Z.H. Ping, J.W. Xie, T.Y. Yu, Permeation of CO_2 through polyurethane, Journal of Applied Polymer Science 40 (7–8) (1989) 1131–1139.
[71] N. Cao, M. Pegoraro, F. Bianchi, L. Zanderighi, Gas transport properties of polycarbonate–polyurethane membranes, Journal of Applied Polymer Science 48 (10) (1993) 1831–1842.
[72] R.D. Raharjo, H.J. Lee, B.D. Freeman, T. Sakaguchi, T. Masuda, Pure gas and vapor permeation properties of poly[1-phenyl-2-[p-(trimethylsilyl)phenyl] acetylene] (PTMSDPA) and its desilylated analog, poly[diphenylacetylene] (PDPA), Polymer 46 (17) (2005) 6316–6324.
[73] B.D. Freeman, Basis of permeability/selectivity tradeoff relations in polymeric gas separation membranes, Macromolecules 32 (2) (1999) 375–380.
[74] L.M. Robeson, Correlation of separation factors versus permeability for polymeric membranes, Journal of Membrane Science 62 (2) (1991) 165–185.